A potential mechanism for abnormal grain growth in Ni thin films on c-sapphire

Dominique Chatain, Blandine Courtois, Saba Ahmad, Gerhard Dehm, Christina Scheu, Clémence Badie, Lionel Santinacci

▶ **To cite this version:**

Dominique Chatain, Blandine Courtois, Saba Ahmad, Gerhard Dehm, Christina Scheu, et al.. A potential mechanism for abnormal grain growth in Ni thin films on c-sapphire. Acta Materialia, 2024, 281, pp.120451. 10.1016/j.actamat.2024.120451 . hal-04731452

HAL Id: hal-04731452
https://hal.science/hal-04731452v1

Submitted on 10 Oct 2024

HAL is a multi-disciplinary open access archive for the deposit and dissemination of scientific research documents, whether they are published or not. The documents may come from teaching and research institutions in France or abroad, or from public or private research centers.

L'archive ouverte pluridisciplinaire **HAL**, est destinée au dépôt et à la diffusion de documents scientifiques de niveau recherche, publiés ou non, émanant des établissements d'enseignement et de recherche français ou étrangers, des laboratoires publics ou privés.

A potential mechanism for abnormal grain growth in Ni thin films on c-sapphire

Dominique Chatain[1]*, Blandine Courtois[1#], Saba Ahmad[2], Gerhard Dehm[2], Christina Scheu[2], Clémence Badie[1+], Lionel Santinacci[1]

[1]Aix-Marseille Univ, CNRS, CINAM, Marseille, France
[2]Max-Planck-Institut für Nachhaltige Materialien GmbH, D-40237 Düsseldorf, Germany

* corresponding author
[#] *now at* Aix-Marseille Univ, Université de Toulon, CNRS, IRD, Mediterranean Institute of Oceanography, MIO, Marseille, France
[+] *now at* Laboratoire des Multimatériaux et Interfaces, UMR CNRS 5615, Univ Lyon, Université Claude Bernard Lyon 1, F-69622 Villeurbanne, France

Abstract

Normal grain growth (NGG) of a (111) textured Ni film on c-sapphire and abnormal grain growth (AGG) of (100) grains at the expense of this (111) texture has been studied as a function of temperature with and without a capping layer. The grain boundaries (GBs) in the Ni film are controlled by the preferred orientation relationships (ORs) adopted by the Ni grains on the sapphire substrate. The 2 variants of a single OR, Ni(111)<1$\bar{1}$0>//Al_2O_3(0001)<1$\bar{1}$00>, form a (111) mazed bicrystal with Σ3 GBs. The (100) grains have a single OR, Ni(100)<010>//Al_2O_3(0001)<1$\bar{1}$00> with 3 variants; their GBs within the (111) grains have the (111)<1$\bar{1}$0>//(100)<010> misorientation.
(100) AGG within the (111) mazed bicrystal of the 100 nm Ni film takes place above 1023 K. The orientation transition is driven by the biaxial elastic modulus anisotropy which favors the growth of (100) grains over (111) grains, as this reduces the elastic strain energy induced by the thermal mismatch between Ni and sapphire. (100) AGG is suppressed and the NGG of the (111) texture is slowed down when the film is covered by a 10 nm amorphous alumina layer aimed at inhibiting surface diffusion. Thus, it is proposed that as long as the surface can act as a sink for the point defects diffusing along the GBs, the movement of the GBs is correlated to the diffusivity of atoms and vacancies, which is a function of their misorientation and crystallographic GB structure.

1. Introduction

Grain boundaries (GBs) in polycrystals control a wide range of material physical properties, which can be modified by grain growth (GG) produced by annealing. Basic understanding of GB motion is a key to controlling the microstructure of a polycrystal, which cannot simply be described as a sum of individual GBs. Indeed, in recent experiments on GG in 3-D, using a non-destructive method, it has been observed that GBs can move against their curvatures [**1**,**2**] unlike a GB in a bicrystal. On the other hand, a recent review of abnormal grain growth (AGG) [**3**] has underlined the lack of understanding of the anisotropy of GB kinetics.
Atomic-scale simulations are able to model the kinetics of GBs, based on disconnection motion [**4**], but this approach is only suitable for analyzing experiments on the motion of a GB in a bicrystal (see for example [**5**]). Today, modelling of GG in polycrystals can only be tackled by a macroscopic approach based on curvature-driven GB motion. In order to better interpret the experimental GB distribution in a microstructure after GG, it has been recently shown that GB stiffness (the second derivative of the GB energy with respect to inclination [**6**]) is more strongly correlated than just GB energy anisotropy [**7**]. This points to the possibility that the motion of a given GB depends on its location in the GB network.

The study of grain growth in thin films is appealing because it deals with microstructures which can be reduced to two dimensions, i.e., consisting of columnar grains. A major experimental issue arises with the fact that at the surface of films, grooving of the emerging GBs and of their triple junctions (TJs) interferes with GB motion as shown recently in [**8**] by simulations. In addition, GB and TJ grooving ends with a complete break-up of the film into separate grains (also called agglomeration) (see [**9,10**] for example). On the other hand, simulations of GG in 2-D microstructures are very flexible since it is possible to check the impact of each parameter/mechanism one at a time, and in particular to ignore the surface of the film and its interface with a substrate. However, an understanding of the mechanisms involved in GG requires the relevant parameters to be implemented in simulations for a reliable prediction and match with experiments.

In order to bridge the gap between experiments and simulations in thin films, and take advantage of the outcome of such an approach in order to better understand the mechanisms involved in AGG, there is a need to design experiments in which the driving forces and mechanisms of GB motion are controlled. This also includes the role of their junction(s) to the external phases (that we name "external line junctions" (ELJs) in order to avoid confusion with the TJs between the GBs in the film).

This paper presents an original set of experiments on GG in thin polycrystalline fcc films, in which the GBs are controlled by using a c-sapphire substrate, and the surface diffusion can be turned on or off by leaving the film surface free or by capping it with an oxide layer, respectively. In a first set of experiments, we observe the evolution of the microstructure of (111) mazed bicrystalline films [**11**], i.e., with only GBs and no TJs, when they are capped or uncapped. We measure the grain boundary length decrease, instead of the averaged grain size increase, to characterize grain growth. In a second set of experiments on uncapped films, we study the abnormal growth of (100) grains, which have 3 orientation variants and grow within the (111) mazed bicrystal.

Such experiments are based on 4 key components:
(1) the control of the film microstructure is achieved by using Ni films on a c-sapphire substrate, such that under annealing, the Ni grains adopt preferred orientation relationships (ORs) which lead to a reproducible GB distribution; (2) the role that the ELJs of the GBs with the film surface play on GG is tackled by comparing the evolution of the microstructure of uncapped films with a free surface to that of films capped by an amorphous alumina layer; (3) the microstructure of the uncapped and capped Ni films is determined by electron backscattered diffraction (EBSD) after annealing at different temperatures; (4) the thickness of the oxide cap is controlled such that at 10 nm, EBSD on Ni can be performed through the cap, and at 30 nm the capping layer can be made to delaminate under annealing, which allows observation of GG on uncapped films after annealing up to 1173 K.

The unexpected outcome of these experiments is that the film microstructure evolves differently depending on whether the film surface is capped or uncapped, i.e., without or with surface diffusion, respectively, that is to say without or with diffusion along the GBs. Normal grain growth (NGG) in a (111) textured film, which is almost a mazed bicrystal, takes place at 873 K in both uncapped and capped films. At temperatures higher than 1023 K, AGG of (100) grains at the expense of the (111) mazed bicrystals, followed by the break-up of the film, occurs in uncapped films. Capping the Ni film, delays its break-up, as expected, but also produces two unexpected phenomena: (1) NGG in the mazed (111) bicrystal slows down and (2) AGG of the (100) grains stops.

Analysis of these results allows the suggestion of a mechanism involved in abnormal and normal grain growth in thin Ni films, that is the diffusion along the GBs coupled to surface diffusion. The efficiency of GB diffusion is controlled by the presence or absence of external sinks for the absorption or emission of the appropriate point defect species (at the surface).

2. Experimentals

2.1. Sample preparation and characterization

Ni film deposition

A 100 nm thick Ni film was deposited on a c-sapphire wafer, 5.08 cm in diameter, purchased from CrysTec GmbH (Berlin, Germany), in an ultra-high vacuum (UHV) chamber. Before deposition the sapphire substrate was annealed at 600 K for 12 h and then cooled down. Deposition of Ni (99.995% pure) was performed at room temperature at a pressure of 6.5×10^{-7} Pa, at a rate of 0.045 nm/sec, by magnetron sputtering.

Annealing conditions

Samples of about 1 cm^2 were cut from the sapphire wafer with the deposited Ni film. They were heat treated at temperatures between 873 K and 1373 K in a 60% Ar + 40% H_2 gas mixture at atmospheric pressure flowing at 10 cc/min, in an alumina tube inserted into a tube furnace. The heating rate to the set temperature was 25 K/min. Cooling from the annealing temperature occurred at the rate imposed by switching the furnace power off (see details in [**12**]). The annealing duration was 1 h for most of the samples. It was 30 mins for the uncapped film annealed at 1173 K.

Capping layer of amorphous alumina

For some of the samples, the Ni film was capped with either 10±1 nm or 30 ±1 nm of an amorphous and continuous alumina layer [**13,14**]. It was deposited by atomic layer deposition (ALD) in a Fiji 200 reactor (Veeco/Cambridge Nanotech) operating with Ar as the gas carrier. The reaction chamber was maintained at 423 K. The deposition conditions have been set according to previous work [**15**]. Al_2O_3 was deposited from trimethylaluminum (TMA from STREM Chemicals, 98%) and deionized water (ρ = 18.2 MΩ·cm) that were stored in dedicated canisters at room temperature. The ALD cycle consisted of sequential pulses of TMA and H_2O separated by purge steps. The pulse and purge durations were 0.06 and 10 s, respectively, for both precursors. Under these conditions, the Al_2O_3 layer growth is 0.068 nm/cycle.

Microstructure analysis after annealing

After annealing the Ni films have either kept their integrity and consist of columnar grains, or they have broken up into separate grains through the well-known mechanism involving GB and TJ grooving at the surface of the film, followed by dewetting of the Ni grains (see for example [**10,16-18**]).

The samples were first observed in a high resolution Scanning Electron Microscope (SEM), Jeol JSM-7900F at 3 kV, and then analyzed using EBSD in a UHV-SEM, to determine the ORs of the Ni grains on the c-sapphire substrate.

The EBSD camera is a "Symmetry" from Oxford Instruments specially built for a home-made UHV-SEM. The electron beam voltage was set at 15 kV and the working distance was chosen between 11 and 15 mm (the maximum field of view is about 1x1 mm^2). The samples were tilted by 68±1° from the horizontal to optimize the electron backscattered pattern (EBSP) quality and the data were processed using the Aztek and HKL Channel 5 software. The investigated regions were scanned with various step sizes from 60 nm to 3 µm depending on the size of the Ni grains, and the acquisition time per point was set between 5 to 20 ms for uncapped films and 100 ms for Ni surfaces capped with a 10 nm of oxide cap. When the capping oxide layer is 30 nm, the Ni EBSP is not accessible through the oxide layer but can be recorded where this oxide layer has detached (delaminated) from the Ni.

Initially, the oxide cap is used for preventing surface diffusion and delays the Ni film break-up [**10**]**.** However, tuning the cap thickness allows us to perform two different experiments. On one hand, when limited to 10 nm, it allows to study grain growth under an oxide cap, without totally shielding the backscattered electrons from the Ni grains; a Ni EBSD pattern forms for reasonably long acquisition times (we can "see" through the oxide cap). On the other hand, a 30 nm oxide film is too thick to allow an EBSD pattern of the Ni film to form, but is useful for studying grain growth in the film at high temperatures; indeed, the grains in the film grow under the oxide cap in the early stages of temperature ramping, and then, the thick cap delaminates due to tensile stress when it crystallizes. GG in these uncapped regions of a pre-grown Ni film can be observed at temperatures where an as-deposited uncapped film would have broken-up.

The Ni film microstructure was characterized by the EBSD scans by using the GB length density, i.e., the length of the GB network normalized by the scanned area (μm/μm^2). It is calculated as the ratio of the average perimeter of the grains and their mean area given by the Aztek software, and is divided by 2 because each GB belongs to two adjacent grains. Only the EBSD scans which contain more than 70% of indexed pixels are used. The EBSD scans were processed so as to replace the unidentified pixels by averaging the neighboring identified pixels. 4 to 7 regions of each sample were measured for obtaining statistically sound data.

3. Results

3.1. Ni film microstructure after deposit

X-ray diffraction (XRD) showed that the as-deposited Ni film had a preferred (111) texture with a few (100) grains, as displayed in Fig. 1a. In Fig. 1b, a transmission electron microscope (TEM) image of a slice of the film, where the grains are colored according to their orientation parallel to the substrate, shows that the deposited film is made up of 20-40 nm nano-grains, consistent with the width of the X-ray peaks. Since the (100) grains are scarce, TEM images cannot provide good statistics of their distribution within the film. The small size of the grains and the randomness of their orientations is probably related to the high energy bombardment at room temperature during magnetron sputtering [**19**].

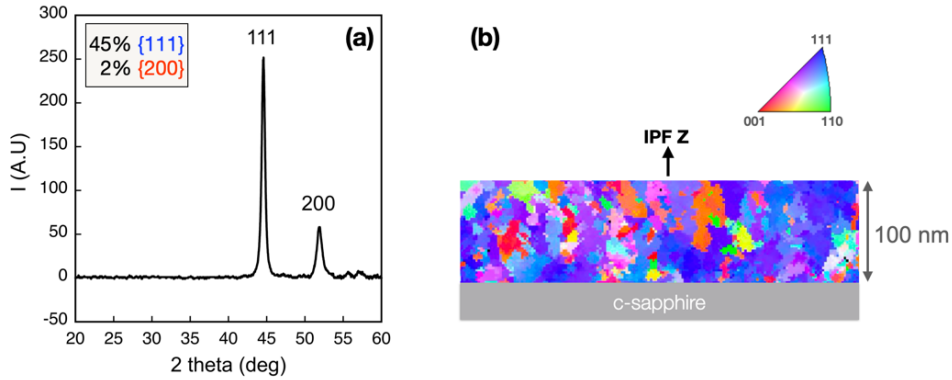

Figure 1. (a) XRD of the as-deposited 100 nm thick Ni film showing the frequency of the {111} and {200} grains that are within ±5° of the perpendicular to the substrate. (b) slice of the film perpendicular to the substrate showing the Ni grains in the film colored according to their plane orientation parallel to the substrate. The color code is given by the standard stereographic triangle (SST) of fcc Ni inset on the top right.

3.2. Orientation Relationships of the Ni grains after annealing

Whatever the morphology of the film after annealing, continuous or broken-up into separate grains, the Ni grains have preferred ORs on c-sapphire. These have been identified by comparing the location of poles of the Ni grains, in a fcc stereogram, to the location of poles in the stereogram of the c-sapphire substrate acquired during the same EBSD run (see Fig. 2). Such an approach allows a resolution of the ORs between the Ni grains and the c-sapphire substrate to better than 0.3°.

The Ni grains have either a (111) or a (100) plane parallel to the (0001) sapphire substrate. They also have preferred in-plane orientations: the <1$\bar{1}$00> and/or the <11$\bar{2}$0> in-plane directions of sapphire (0001) are parallel to the <1$\bar{1}$0> interfacial in-plane direction of the (111) Ni grains, and to the <010> in-plane direction of the (100) Ni grains. The 3 ORs have several variants because of the symmetry of the abutting Ni and sapphire planes. They may be written as follows:

OR1 (2 twinned variants) displayed in Fig. 2b:
Ni{111}<1$\bar{1}$0> // Al_2O_3(0001)<1$\bar{1}$00>

OR2 (2 twinned variants) displayed in Fig. 2c, with a variable angular deviation from the perfect in-plane direction alignment:
Ni{111}<1$\bar{1}$0> // Al_2O_3(0001)<11$\bar{2}$0> within ±7°

OR3 (3 variants) displayed in Fig. 2d, with a variable angular deviation from the perfect in-plane direction alignment:
Ni{100}<010> // Al_2O_3(0001)<11$\bar{2}$0> and <1$\bar{1}$00> within ±4°

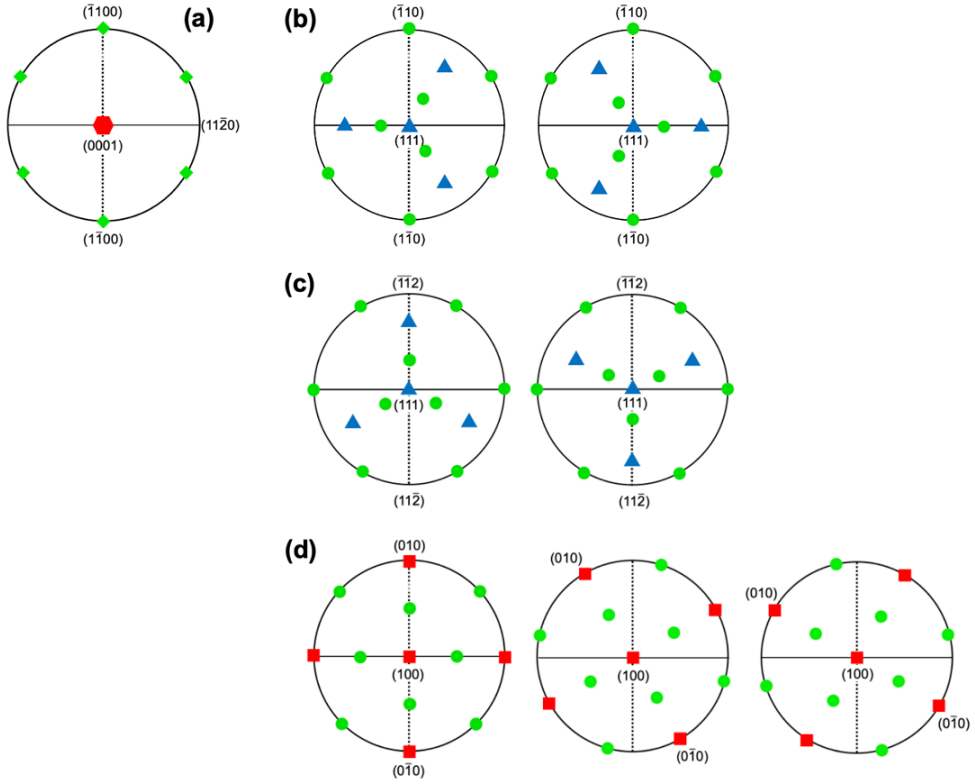

Figure 2. Parallel stereograms of sapphire and Ni in the 3 orientation relationships, showing the poles in the northern hemisphere. (a) The trigonal sapphire stereogram centered on the (0001) pole (red hexagon) contains the 6 in-plane {1$\bar{1}$00} poles (green lozenges) located on the outer circle of the stereogram. One of the (11$\bar{2}$0) poles at 30° from the {1$\bar{1}$00} is also shown. (b) and (c) are the fcc stereograms of Ni(111) in OR1 and OR2, respectively, displaying their two variants; they are centered on a (111) pole (blue triangle) and display the 3 other {111} poles; the 9 {110} poles (green circles) are plotted such that 6 are superimposed on the {1$\bar{1}$00} and the {11$\bar{2}$0} poles of sapphire, respectively. (d) Shows the fcc stereograms of Ni (100) in OR3 with its 3 variants; they are centered on a (100) pole and display 4 other {100} poles which are superimposed on the {1$\bar{1}$00} poles of sapphire. In these 3 stereograms, the 8 {110} poles (green circles) are also plotted.

3.3. Microstructure, morphology and grain boundaries of the annealed Ni film

The Ni films adopt two types of microstructures and morphology depending on the annealing temperature, the ORs of the Ni grains after annealing, and the presence of a capping oxide layer. They are reported in Figs. 3, 4, 5 and 7 and commented below.

Microstructure (1): (111) mazed bicrystal

After annealing at 873 K, the collection of nano-grains of the as-deposited Ni film displayed in Fig. 1b has recrystallized into (111) textured columnar grains consisting of a mazed OR1 bicrystal with up to 10% of OR2 grains, as shown in Figs. 3a and 3b for a 10 nm oxide capped and an uncapped film, respectively. The capping oxide does not change the microstructure, i.e., the ORs of the Ni grains, their distribution and their GBs are identical, but it produces a decrease of the rate at which the grains grow. The GB length density is significantly longer by almost a factor of 1.5 when surface diffusion is stopped by the capping layer. It is 1.94±0.33 μm/μm^2 and 2.88±0.31 μm/μm^2 for the uncapped and capped films, respectively, as reported in Fig. 6. This means that suppressing surface diffusion was more efficient in slowing grain growth than the grooving of the GBs at the external line junction (ELJ) formed where the GBs intersect the free surface of the uncapped films.
The GBs have been identified using the Aztek EBSD software (assuming that they are perpendicular to the film surface). They are Σ3 GBs between the two OR1 (twinned) variant grains. The GBs between the OR1 and OR2 grains, which are not all exactly rotated by 30°, are mainly Σ7, Σ13b, Σ19b, or Σ21a.

The Σ13b and Σ21a have the highest frequencies. These results are similar to those previously found for Cu and Al on c-sapphire [**20-22**].

The morphologies of the Ni films capped with a 10 nm oxide layer after annealing at 1273 K and 1373 K, are shown in Figs. 4.
At 1273 K, the mazed bicrystal film has grown self-similar grains bigger than the ones grown at 873 K (Fig. 3a) such that the GB length density has decreased (see Fig. 6). Holes extending down to the sapphire substrate have formed (white regions in Fig. 4a). They are not located at the TJs of the GBs of the OR2 grains embedded in the mazed OR1 bicrystal, but rather at the GBs above which the capping oxide had delaminated.
At 1373 K, the capped film has broken-up into finger-like grains (Fig. 4b). This morphology results from the fractal growth of holes propagating along the GBs parallel to the substrate rather than the grooving of the GBs perpendicular to the surface [**10**]. The finger grains consist mostly of the two OR1 variants. Their size is related to the grain size before fragmentation of the film. The smallest grains formed during the dewetting process have shrunk and fed the larger ones by Ostwald ripening.

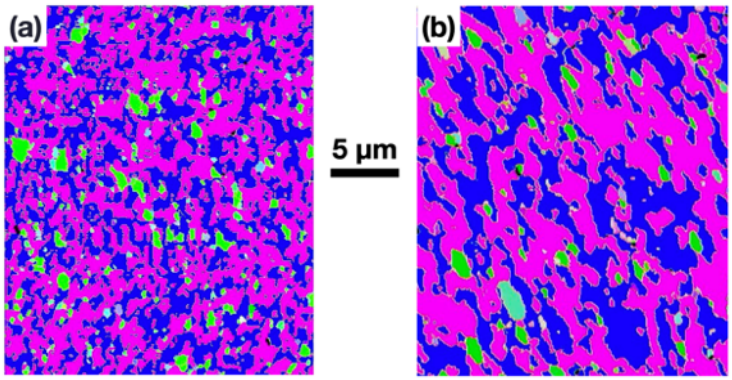

Figure 3. False color EBSD images of (111)-textured Ni films after annealing at 873 K, (a) with and (b) without a capping oxide layer. The self-similar microstructures consist of OR1 bicrystals together with a few OR2 grains; the two twinned variants of the OR1 grains are blue and purple and the OR2 grains are in shades of green.

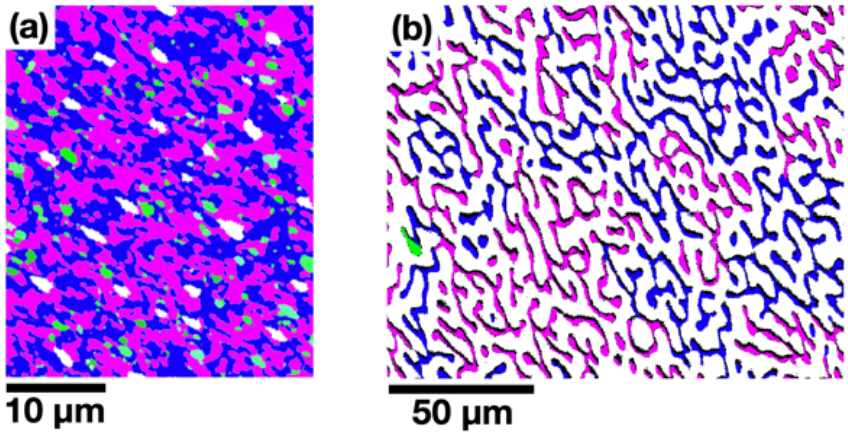

Figure 4. False color EBSD images of the microstructure of Ni films capped with a 10 nm alumina film, after annealing at (a) 1273 K and (b) 1373 K. As in Fig. 3, the OR1 variant grains are blue and purple and the OR2 grains are colored in different shades of green. The sapphire substrate is white.

Two samples capped with 30 nm of amorphous alumina were annealed at 1173 K and 1273 K. The oxide layer is too thick to obtain an EBSD pattern from the Ni underneath. However, after the mazed bicrystals have formed under the capping layer during the ramping-up of the temperature, the Ni film surface is freed in some regions because the alumina layer which crystallizes above 873 K [**16**], has delaminated and detached as a result of stresses. This is illustrated in Figs. 5 in the case of the sample annealed at 1273 K. The microstructure of the (111)-textured Ni film in these alumina free regions is self-similar to that shown in Figs. 3 and 4a, with larger grains overgrown after the surface has been freed.

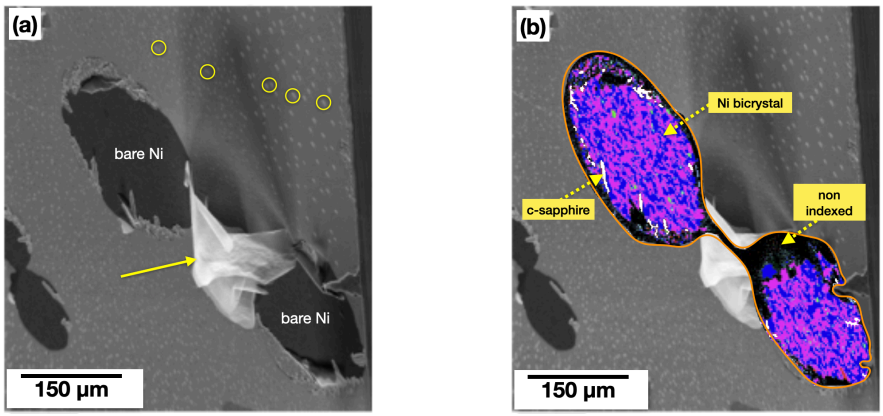

Figure 5. Oxide cap delamination on a film initially covered with 30 nm of alumina, after annealing at 1273 K. (a) secondary electron (SE) image with two large black elliptic regions where the Ni film has been freed from the alumina layer (bare Ni). The alumina cap has not completely detached from the sample. It is visible as a crumpled white veil (see arrow) hanging off the surface between the two elliptical black Ni regions. The grey capping layer, around these features, is still attached to the Ni film, except where there are light grey "blisters/bubbles"; several of them are circled on the top right of the image; (b) surrounded with an orange line, false color EBSD map of the Ni microstructure in the two bare Ni regions, superimposed on the SE image; the Ni film is a mazed bicrystal of the two OR1 blue and purple variants with a few OR2 grains in shades of green. The black regions located around the colored grains are not indexed because the Ni film is shielded by the thick alumina capping layer; the white elongated regions at the periphery of the colored grains correspond to the sapphire substrate at the bottom of holes, opened in the Ni film which has started to break-up/dewet.

The GB length density in the Ni film, with and without an alumina cap, after annealing at different temperatures, is reported in Fig. 6.
The GB length density of the capped films (with brown error bars), fitted with a brown dashed line, decreases and plateaus as the annealing temperature increases.
The GB length density of uncapped films have blue or green error bars. The film annealed at 873 K (blue error bar) has remained continuous, however at higher annealing temperature, the uncapped film has broken up. Thus, the points with green error bars have been measured on Ni in delaminated regions of samples initially covered with a 30 nm oxide layer (see Fig. 5). The GB length density of uncapped films drops and keeps decreasing as the annealing temperature increases as indicated by the dashed blue line, i.e., grain growth is faster when the surface is uncapped even if GB grooving is activated.

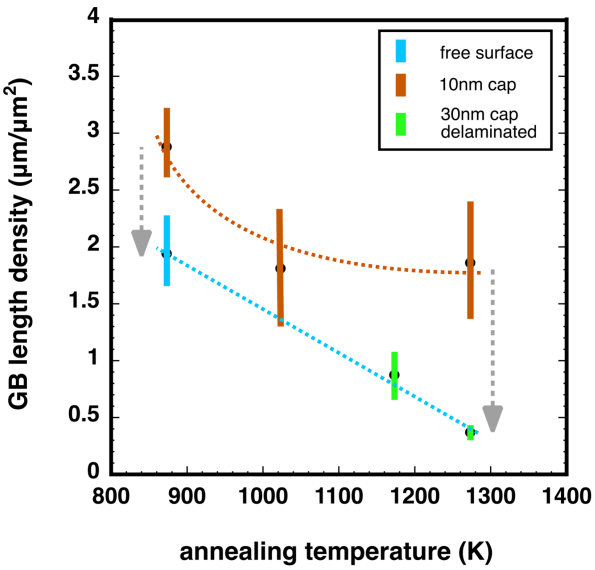

Figure 6. GB length density with standard deviation measured on several (4 to 7) scans as a function of the annealing temperature for 3 capped and 3 uncapped samples. The 2 points on the blue dashed line, with a green error bar have been measured on Ni regions of a Ni film initially covered with 30 nm of alumina where the oxide layer has delaminated during annealing (as illustrated in Figs. 5). The dashed brown line joining the data for capped films and the dashed blue line through the uncapped samples are guides for the eye. The two grey vertical arrows on the sides emphasize the drop of the GB length density when the Ni film surface is free of a capping layer.

Microstructure (2): small (111) and very large (100) grains

Uncapped films annealed at 1023 K and 1173 K have broken-up into micron-sized (111) grains and large (100) single- or poly-crystals with sizes that span from 100 µm up to 1 mm. Their orientations have been checked using EBSD. Figs. 7 display these two kinds of grains. The (111) grains are fairly homogeneously distributed while the (100) grains appear in uncorrelated locations of the sample and with different shapes. They can appear as an isolated (100) single-crystal or be gathered into a (100) oligocrystal, i.e., polycrystal made of grains with the same surface orientation. They are always in a "sea" of (111) tiny grains. Such an inhomogeneous distribution is often the signature of AGG. Figs. 7 show the different configurations and shapes of the (111) and (100) grains in SE images and EBSD maps.

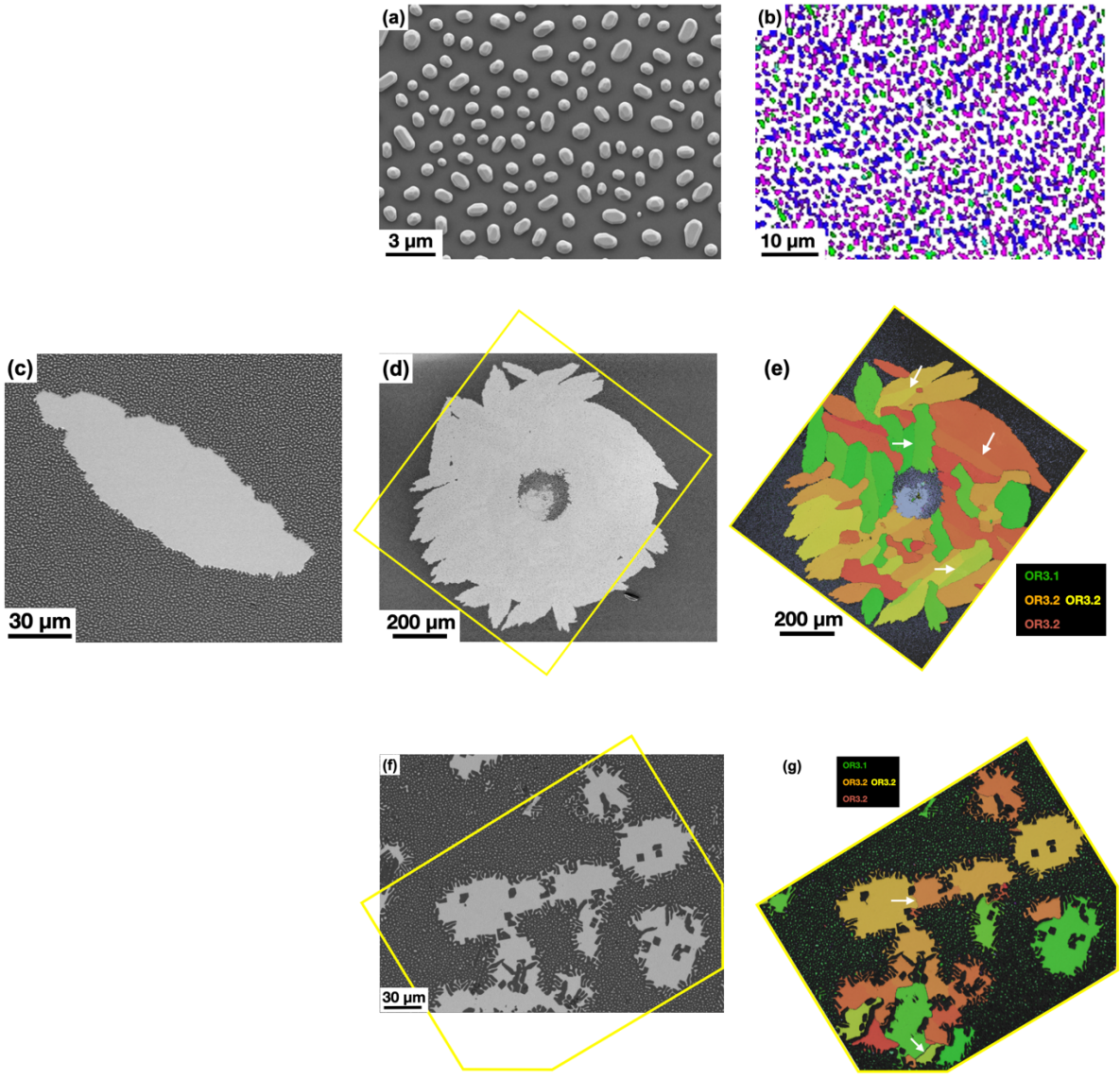

Figure 7. Secondary electron (SE) and EBSD maps of uncapped Ni film broken-up into small (111) and large (100) grains after annealing at 1023 K and 1173 K. On the SE images, the Ni grains appear in light greys, and the sapphire substrate in dark greys. (a) faceted crystals with (111) orientations parallel to the sapphire substrate (b) EBSD map of the same region at a smaller magnification in false colors (white for the sapphire substrate, purple/blue for the OR1 Ni grains and green for the OR2 Ni grains). (c) a (100) single-crystal within a "sea" of (111) grains (shown in (a)) abnormally grown at 1023 K; (d) a (100) poly-crystal abnormally grown at 1023 K within a "sea" of tiny (111) grains barely visible because of their size; (e) EBSD map of part of the (100) polycrystal shown in (d), where the grains have colors depending on their in-plane orientation corresponding to the 3 (100) variants to the sapphire substrate. (f) SE image of large (100) grains abnormally grown at 1173 K within a "sea" of tiny (111) grains barely visible because of their size; (g) EBSD map of a region of the image shown in (f). All the (100) grains have only 3 possible orientations OR3 within ±4°. The GBs between the (001) grains are either between 2 of the OR3 variants or low angle boundaries between two grains with a few degrees of deviation (white arrows display some of them).

In the regions where the film microstructure was a mazed (111) bicrystal, grooving has separated the finger-shape (111) OR1 grains which then broke-up by Rayleigh instability into strings of beads as detailed in [**18**]. These (111) grains are present in all the images of Figs. 7a, c, d, f but barely visible in c, d and f because of their tiny sizes compared to the size of the (100) grains. In the SE image of Fig. 7a, it is seen that the (111) bead grains are facetted single-crystals. Their ORs are displayed in an EBSD map at lower magnification in Fig. 7b with the false colors used earlier to identify the OR1 and OR2 variants. Strings of bead-crystals of the same variant correspond to the former finger shaped grains.

Figs. 7c, 7d and 7f are secondary electron images showing the different distributions of the (100) grains of the three OR3 variants within the "sea" of (111) micron-sized bead grains. The growing shapes of the (100) grains were "frozen" when they were separated from the (111) grains by GB grooving. The misorientation of these GBs between the OR1 (111) and OR3 (100) grains before the break-up was (100)<010>//(111)<1$\bar{1}$0>.

The (100) grains grown in the samples annealed at 1023 K and 1173 K have different shapes. At 1023 K, an isolated (100) single-crystal shown in Fig. 7c has a lens shape, elongated in a <010> direction along which it has grown the fastest. The elongation is related to the inclination of the ex-GBs between the (100) OR3 grains and the (111) mazed bicrystal. This is deduced from EBSD map/pole figures on both kinds of crystals (not shown here) (see more details in Fig. 8a). The (100) grains with free edges at the periphery of the big (100) polycrystal of Fig. 7d also have lens shapes elongated in the 3 equivalent <010> directions at 120°, corresponding to the 3 OR3 variants of Ni on the sapphire substrate. When the growing (100) grains contact each other, new GBs form. This is displayed on the EBSD maps of Fig. 7e which corresponds to the large (100) polycrystal of Fig. 7d. The (100) grains in the polycrystals in (e)/(f) have different colors corresponding to the 3 (100) variants. Because the variants can deviate by ±4°, some of the GBs are low angle GBs. Some of them are marked with white arrows in the EBSD map of Figs. 7e and 7f.
At 1173 K, the free edges of the (100) grains have a more rectangular shape. During the annealing first the GBs between the (100) and (111) grains disappear. Then the free edges of the (100) crystals start to dewet and tend to develop <010> edges as observed in [**17**] for Ni(100) films dewetting from MgO in the same gas environment as used in the current experiments.

Fig. 8a shows a sketch of a polygonal (100) grain within the (111) matrix, delimited by 3 kinds of GBs, presumably perpendicular to the substrate, and having the misorientation between OR1 and OR3 determined by EBSD. It is a simplified shape of the nuclei that develop into the (100) lens-shaped grain shown in Fig. 7c. The abutting planes of these 3 GBs are made up of two perpendicular (010) and one (110) planes on the side of the (100) grain (denoted $(010)_{100}$, $(001)_{100}$ and $(110)_{100}$), which face the two perpendicular $(\bar{2}11)_{111}$ and $(1\bar{1}0)_{111}$ planes and a plane close to $(\bar{4}3\bar{1})_{111}$ of the (111) grain, respectively. The longest GBs $(001)_{100}//(1\bar{1}0)_{111}$ are made up of two low index facing planes. The two other GBs with low indices on the side of the (100) grain face high index planes, namely $(\bar{2}11)_{111}$ and ~$(\bar{4}3\bar{1})_{111}$ planes, on the side of the (111) crystal; these GBs move faster than the $(001)_{100}//(1\bar{1}0)_{111}$ GB and eventually disappear, as has been seen for the fast moving planes of crystal Wulff shapes [**23**].

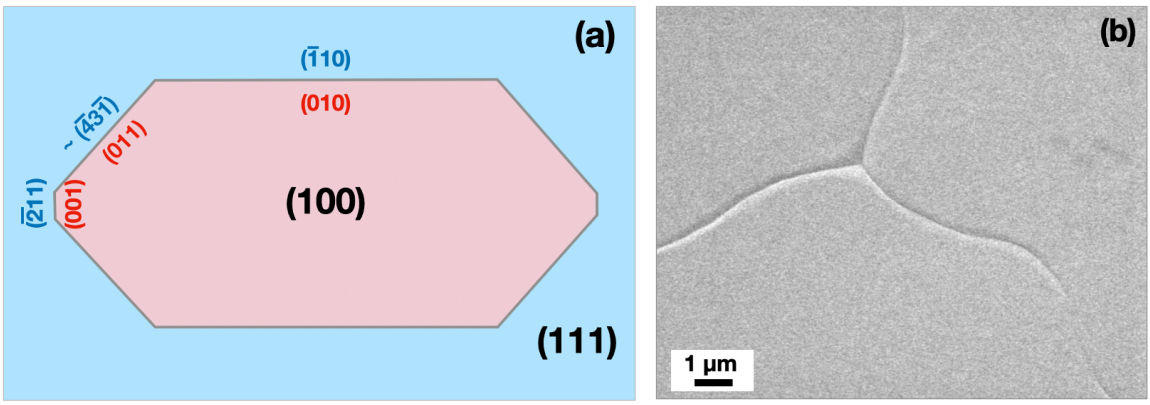

Figure 8. (100) OR3 grains and their GBs. (a) Sketch of an elongated (100) grain in a mazed (111) OR1 bicrystal surrounded by three GBs with low index planes on the edges of the (100) grain (in red) facing the corresponding planes in the (111) grain (in blue) according to the misorientation between OR1 and OR3; (b) SE image of three (100) OR3 grains with their grooved GBs meeting at 120° at a triple junction (sample annealed at 1173 K). Grooving varies depending on the GB inclination as seen along the rightmost GB where a part of the GB is almost ungrooved.

During growth of two (100) grains of 2 of the 3 variants can merge and form a GB. It has a unique misorientation, since the 3 variants are rotated by 120° from each other, as found for the (100) grains of an Al film deposited on Si(111) [**24**]. The secondary electron image of Fig. 8b shows the meeting of 3 (100) grains of the 3 variants. Their GBs meander and have anisotropic grooving depending on the GB inclination. Fig. 8b also shows a TJ formed by these 3 GBs at 120°, where grooving is deeper, as expected [**9,25**].

4. Discussion

4.1. Orientation relationships

The OR of fcc metals on ionic solids, which are weakly bonded phases, has been studied in several systems. On cubic ionic substrates, it was found that atomic matching of the fcc metals was not a necessary condition for an OR to be preferred [**26**]. Instead, the alignment of the densest planes and their densest in-plane rows has often been observed, and is referred to as the lock-in model [**27**]. Since the interface energies do not correlate with the density of coincidence or lock-in sites [**28**], many studies have suggested that lattice mismatch could be a key parameter in the resulting OR.
After annealing, the Ni grains in the present study have adopted 3 preferred ORs with either a (111) or a (100) plane parallel to the substrate. It is very unlikely that Ni grains randomly oriented in the deposited film could rotate to adopt these ORs. Instead, it appears that the growth of preferred seed-grains in contact with the substrate has been activated by relevant driving forces and mechanisms. The 3 kinds of seeds with preferred ORs are probably present because of the high energy deposition technique. Physical vapor deposition (PVD) by thermal evaporation or electron beam sputtering favors growth of (111)-textured columnar seeds from which only OR1 and OR2 grains are preferred to grow during annealing. This has been observed in the case of Ni films deposited by PVD and annealed at 1625 K (0.94 $T_{melting}$) [**29**] and of Ni films deposited by magnetron sputtering and annealed at 773 K (0.46 $T_{melting}$) [**30**].

Development of OR1 agrees with the lock-in model [**27**] since the densest <1$\bar{1}$0> atom rows of Ni(111) align with the densest <1$\bar{1}$00> ion rows of the (0001) sapphire plane. Because there are two Ni OR1 twinned variants, the Ni film microstructure is a mazed bicrystal with no triple junctions. This is consistent with the observations that OR1 has been found in the growth of several fcc metals and alloys on ionic solids [**16,20,21,29-34**]. The range of lattice mismatches of these fcc phases with the c-plane of sapphire being large, the two abutting lattices must be accommodated by localized or delocalized dislocations, as suggested in the case of Cu [**20**].

OR2 is such that the densest <1$\bar{1}$0> row of Ni(111) aligns with the second densest in-plane direction, <11$\bar{2}$0> of Al_2O_3(0001). However, the OR2 Ni grains display a range of angular in-plane deviation of about ±7° from the exact alignment, as has been observed for several other fcc phases such as Al [**16,21**], Cu [**20,33**], Pt [**31**] and high entropy alloys (HEA) [**34**]. It has been suggested in the case of Al [**16**] that the deviation from OR2 allows an optimization of the GB misorientation between OR1 and OR2. The Σ13b and Σ21a GBs found with the highest frequency in Ni, correspond to OR1-OR2 misorientations where OR2 grains deviate by 2° and 8°, respectively. Considering that the interface bonding is weak, GB energy or mobility could favor the growth of misaligned OR2 grains within the OR1 mazed bicrystal. Further investigation of the GBs between two twist (111) GBs with these misorientations are necessary in order to verify this hypothesis.

OR3 is the most puzzling OR because the two perpendicular in-plane rows of Ni(100) parallel to the densest directions of (0001) sapphire (<1$\bar{1}$00> and <11$\bar{2}$0>) are <010>, i.e., not the densest <110> directions. OR3 has recently been found in fcc HEA films [**35**] also prepared by magnetron sputtering. An equivalent of OR3 named "twist orientation" (i.e., rotated in-plane by 45°) has been mentioned for fcc metals on cubic ionic substrates [**28**]. However, there have been reports that fcc (100) planes grown on a 3-fold symmetry (111) substrate, align their densest <011> directions. This is the case for Al(100) on Si(111) [**24**] and for Ag(111) on Ni(100) [**36-39**], both interfaces between weakly bonded phases. In a review on (100)/(111) interfaces [**40**], it has been suggested that the d-spacing criterion proposed by Wolf [**41**] which requires low-index planes to lie parallel to the interface is a unique attribute that favors the stability of such interfaces.
The d-spacings of {010} and {011}/{022} in a Ni(100) plane are 0.176 nm and 0.124/0.248 nm, respectively, while for {3$\bar{3}$00} and {11$\bar{2}$0} in an Al_2O_3 (0001) plane, they are 0.137 nm and 0.238 nm, respectively [**42**]. Matches of <010> direction of Ni(100) and the two <1$\bar{1}$00> and <11$\bar{2}$0> in an Al_2O_3 (0001) plane is poor, under compressive and tensile strain, respectively:

$d<010>_{Ni(100)}$-$d<1\bar{1}00>_{Al2O3(0001)}/d<010>_{Ni(100)}$ = -0.22
$d<010>_{Ni(100)}$-$d<11\bar{2}0>_{Al2O3(0001)}/d<010>_{Ni(100)}$ = +0.26
On the other hand, a <011>/<022> direction of Ni(100) better matches the <1$\bar{1}$00>/<11$\bar{2}$0> direction of sapphire with only a compressive strain of Ni in the <1$\bar{1}$00> direction:
$d<220>_{Ni(100)}$-$d<1\bar{1}00>_{Al2O3(0001)}/d<220>_{Ni(100)}$ = -0.1
$d<110>_{Ni(100)}$-$d<11\bar{2}0>_{Al2O3(0001)}/d<110>_{Ni(100)}$ = +0.04

The d-spacing of the two abutting crystals does not explain OR3. Interface reconstruction as observed for OR1 with Ni [**29**] could be envisaged. However, the GB energy between OR3 and OR1 could be a better explanation as suggested for the growth of the OR2 grains within an OR1 film [**16**].

The technique used to deposit the Ni film has allowed the growth of tiny OR3 seeds of Ni in contact with the sapphire (see Fig. 1). The driving force to overgrow these OR3 grains at the expense of the (111) OR1 grains, is explained in the next section.

4.2. Abnormal and normal grain growth: driving force and mechanisms

When a 100 nm thick Ni film on c-sapphire is annealed at 873 K (0.52 $T_{melting}$), it recrystallizes into a (111) texture. At and above 1023 K (0.64 $T_{melting}$), AGG of (100) grains takes place at the expense of this (111) texture, before the film breaks-up; the GBs between the (100) and (111) grains have moved several tens of times faster than those between the (111) grains. This requires a driving force and a mechanism. It is worth mentioning that the film is subject to a volumetric driving force upon annealing because the thermal expansion of sapphire is smaller than that of nickel.
In this section, GG kinetics in the Ni film are discussed. First, the driving force responsible for the (100) grain growth at the expense of a (111) texture is addressed, then GG kinetics in the (111)-textured film with and without an oxide capping layer is analyzed. Finally, a possible mechanism for AGG of the (100) grains at the expense of the (111) texture involving diffusion along the GBs is proposed.

Driving force for the growth of (100) grains at the expense of a (111)-textured film

The driving force of the transition from (111) to (100)-textured films has been extensively studied in Cu and Ag films of thickness ranging from 50 nm to several microns (see for example [**36,43-46**]), either on single-crystal [**43**] or on amorphous [**44,46,47**] substrates. It is described in the model of Thompson and Carel [**44,45**] as the result of a reduction in elastic energy when the grains switch from a (111) to a (100) orientation, which overcompensates the surface energy increase when (100) replaces (111) surfaces. This model infers that the grains are elastically strained in the plane of the film. The thinner the film, the higher the strain required to balance the surface/interfacial energy force per unit of volume [**44,45**]. Thus, given the stress, there is a minimum thickness above which the (111) to (100) transition occurs. On the other hand, the thinner the film, the larger the elastic strain its grains can sustain before yielding [**44,48,49**].

The values of the C_{11}, C_{12} and C_{44} elastic moduli of Ni are equal to 249, 155 and 114 GPa, respectively [**50**]. The degree of elastic anisotropy is expressed by the Zener anisotropy ratio $A = (C_{11}-C_{12})/C_{44}$. A is 2.5 for Ni, slightly lower than for Ag (3.0) or Cu (3.2). Thus the (100)-(111) transition should also occur in Ni films, under appropriate conditions of film thickness and stress imposed on the film.
Our experiments deal with 100 nm Ni films on c-sapphire, annealed at temperatures higher than the deposition temperature by ΔT. Upon annealing, a compressive thermal stress, ε_T, is implemented in the Ni film. $\varepsilon_T = \Delta\alpha_{Ni/Al2O3}\,\Delta T$, where $\Delta\alpha_{Ni/Al2O3} = 4.9\ 10^{-6}\ K^{-1}$ is the difference in thermal expansion coefficient between nickel and sapphire, and is positive, ($\alpha_{Ni} = 13.4\ 10^{-6}\ K^{-1}$ [**51**] and the average value of $\alpha_{Al2O3} = 8.5\ 10^{-6}\ K^{-1}$ [**52**]). The elastic energy reduction and the surface energy cost, when a (100) grain replaces a (111) grain in a 100 nm thick film are calculated below.
The biaxial elastic moduli of the (100) and (111) surfaces of Ni may be written as a function of the C_{ij} coefficients (see for example [**53**]):

$M_{100} = C_{11}+C_{12}-2C_{12}^2/C_{11} = 211$ GPa and $M_{111} = 6C_{44}(C_{11}+2C_{12})/(C_{11}+2C_{12}+4C_{44}) = 377$ GPa Eqs. 1

The lateral strain energy densities, W_{hkl} for the (100) and the (111) planes are related to the biaxial stress, ε, and their biaxial elastic modulus, M_{hkl}, by the following equation:

$W_{hkl} = M_{hkl}\,\varepsilon^2$ Eq. 2

Using the values of M_{100} and M_{111} calculated in Eqs. 1, the elastic energy reduction when a Ni(111) surface is replaced by a Ni(100) surface is:

$$\Delta W = W_{111} - W_{100} = 166\ \varepsilon^2\ \text{GPa} \qquad \text{Eq. 3}$$

On the other hand, the energy cost in surface energy, γ^s, and interfacial energy, γ^i, is:

$$\Delta G\gamma = 1/h\ [(\gamma^i_{100} - \gamma^i_{111}) + (\gamma^s_{100} - \gamma^s_{111})] \qquad \text{Eq. 4}$$

$\Delta G\gamma$ has the units of pressure because the surface and interfacial energy contributions are divided by the film thickness (h = 100 nm). The interfacial energy anisotropy is set to zero for Ni on c-sapphire as observed for Cu on c-sapphire [**54**]. The surface energy anisotropy is of the same order of magnitude for fcc metals [**55-58**]. The Ni surface energy, $\gamma^{Ni(s)}$, is isotropic close to the melting point (0.88 and 0.95 $T_{melting}$) [**55**]. $\gamma^{Ni(s)}_{100}$ is about 9% larger than $\gamma^{Ni(s)}_{111}$, as seen on the Ni crystal shape equilibrated at 1253 K (0.74 $T_{melting}$) in [**18**]. With $\gamma^{Ni(s)}$ equal to 1940 mJ/m^2 at 1800 K [**59**], and a temperature coefficient of -0.35 mJ/m^2/K measured for liquid Ni [**60**], $\gamma^{Ni(s)}$ is 2220 mJ/m^2 at 1000 K. Thus, $\Delta G\gamma \sim 2$ MPa.

Equating ΔW and $\Delta G\gamma$, it is found that the biaxial strain necessary to supersede the surface energy cost must be larger than $\varepsilon^* = 3.5\ 10^{-3}$. The thermal strain due to the thermal expansion coefficient difference between Ni and sapphire is $\varepsilon_T = 4.9\ 10^{-6}\ \Delta T$. At 873 K ($\Delta T$ = 580 K), where only a (111) texture film had formed, $\varepsilon_T = 2.8\ 10^{-3}$, below ε^*. At 1123 K (ΔT = 730 K), where the (111)-(100) transition is observed, $\varepsilon_T = 3.6\ 10^{-3}$, i.e., slightly above ε^*. The compressive stress built-up in the film during deposition [**61**] may also add to the thermal strain. Thus, the elastic biaxial strain can actually be the driving force for the observed growth of the (100) grains in the (111) texture.

Carel [**47**] investigated the (111)-(100) orientation transition in a Ni film supported on an amorphous silica layer grown on a Si wafer of thermal expansion $\alpha_{Si} = 2.6\ 10^{-6}\ K^{-1}$, i.e., on a substrate where $\Delta\alpha_{Ni/Si}$ ($9.8\ 10^{-6}\ K^{-1}$) is twice $\Delta\alpha_{Ni/Al2O3}$. For 100 nm thick films deposited at room temperature, the transition was found to occur for $\Delta W \sim 5$ MPa, i.e., at ΔT = 460 K, which is about 2/3 of the one found when Ni is stressed by sapphire. This is consistent with our results since the experiments in [**47**] used X-ray diffraction to identify the occurrence of the transition at a ratio of (100) to (111) Ni grains equal to 1. This technique is not suitable to identify the scarce occurrence of large (100) grains, such as the one observed in the present experiments.

The transition from (111) to (100) grains could have been missed had the (100) grains not grown abnormally, because: (1) the quantity of as-deposited (100) seeds in contact with the substrate which grow in OR3 is below 2% of (100) grains identified by X-ray (cf. Fig. 1), and (2) above 1073 K (0.62 $T_{melting}$), Ni surface diffusion is fast enough [**62-64**] for a 100 nm Ni polycrystalline film to start to break-up into separate grains within 30 mins [**12**].

An oxide layer was deposited on the Ni film to suppress surface diffusion and delay film break-up due to GB grooving. The purpose was to follow GG in continuous films at temperatures higher than 1023 K. For oxide layers less than 10 nm thick, tested on Cu films, amorphous Al_2O_3 has been found to be the most efficient to prevent grooving [**59**]. A native alumina layer formed on Al films has indeed prevented dewetting of 250 nm thick Al films on c-sapphire annealed at 0.94 $T_{melting}$(Al) for several tens of hours [**16**], and has also avoided impeding of GB motion during GG of Al bicrystals between 0.52 and 0.97 $T_{melting}$(Al) [**66,67**]. However, we found that the capping oxide layer had suppressed the growth of the (100) grains in the Ni(111) textured film. This was unexpected because the driving force for (100) growth, i.e., the Ni elastic strain anisotropy, is still present, the surface energy penalty had been strongly reduced and the important effect of minimizing the energy of the film-substrate interface is not affected. The analysis of grain growth in the (111) textured film, presented below, provides insight into the mechanism involved in GG of a strained film.

Grain growth in the (111) textured film

Upon annealing, the grains of the mazed OR1 bicrystal, containing a few OR2 grains, grow larger and retain the same microstructure (i.e., self-similar) for both capped and uncapped samples. Two important features displayed in Fig. 6 need to be addressed: (1) GG is slower in capped films compared to uncapped films and (2) the GG rate tends to stagnate above 1023 K (0.61 $T_{melting}$) when the film is capped.
The capping alumina layer could contribute to enhance GG, because when it crystallizes above 873 K [**16**], it adds an extra stress in the film, which may be significant at the interface [**68**]. This would add to

the compressive stress due to thermal expansion mismatch with the substrate. Since we observe a decrease of GG rate when the film is capped, another explanation for GG rate decrease due to the capping layer is proposed below.

GG participates in the release of the compressive strain produced in the film during deposition and annealing, and diffusion mechanisms are involved in the kinetics of this process. Since diffusion within the GBs is faster than in the bulk, the GBs act as short-circuit paths for the diffusing species. As these species merge at the surface where diffusion is faster than at GBs, they spread out.
When surface diffusion is stopped by the capping layer, the species diffusing along the GB get stuck when they reach the surface, which no longer acts as a sink or a source for the diffusion processes. Thus, the mechanism involving diffusion short-circuit is no longer involved in GG and we observe that GG slows down. This means that diffusion along the GB participates in GG. This is consistent with the activation energy of GB kinetics measured in thin Ag films which suggests that surface diffusion is involved in GG [**69**]. Also, in [**70**] it is suggested that diffusion along GBs is the mechanism of GG in thin Ni films deposited on amorphous SiO_2.This conclusion is supported by finding that the activation energy for GG is comparable to that for self-diffusion of Ni in GBs. It also agrees with the analysis of Kobrinsky and Thompson [**71**] showing that surface diffusion to and down GBs, whose spacing scales with film thickness, mediates strain accommodation in uncapped films. It also fits the results of [**67**] regarding the motion of the GBs of a bicrystal under shear stress, which suggests that low angle GBs (LAGBs) need bulk diffusion to move, while high angle GBs (HAGBs) need diffusion along the GB. Finally, it is also consistent with the observation of hole formation at the GBs of Cu films under tension, when they are covered with an alumina layer [**72**]: the vacancies accumulate at the GBs because they cannot be evacuated when they reach the surface.

Thus, the results confirm previous research and suggest that for capped films, the strain energy of the film is likely released by bulk diffusion at temperatures above half the Ni melting point [**73**].

Mechanism involved in the AGG of the (100) grains: relative GB kinetics

When annealing at and above 1023 K begins, GG is fast enough to overcome GB grooving. As the strain energy is consumed GG slows and GBs get pinned by grooving at the surface. This proceeds until the film breaks-up. Above a certain size, the grains yield such that the strain can also be released plastically.
In order to have AGG, the GBs surrounding the grains growing abnormally should move faster than the GBs between the other grains [**3**]. In our experiments, the GBs between (100) and (111) grains move faster than the Σ3 GBs between the (111) variants of the OR1 grains.
The necessary driving force for AGG is the anisotropy of strain energy, i.e., the equivalent of a higher "chemical potential" in the (111) than in the (100) grains, and all the (111) grains are at the same "chemical potential". To release the compressive stress in the film with small grains, Ni atoms are likely to self-diffuse along short-circuit paths such as the GBs, up to the surface where they are dispersed by surface diffusion: the limiting rate of this process is the diffusion along the GBs when the surface is free because surface diffusion is faster than GB diffusion. The GBs which are the most "disordered" are those along which diffusion is the fastest. Thus, it is likely that the GBs around an OR3 (100) grain move the fastest because of their structure, and of the driving force for replacing (111) grains by (100) grains. When the surface is capped, the atoms cannot diffuse along the GBs at a rate limited by GB diffusion because the surface has become an interface along which diffusion is slower than along GBs. Thus, diffusion along the GBs can no longer relieve the strain and all the GBs move at about the same speed. While there is still an advantage to grow the (100) grains, there is no longer a mechanism available to be used for their abnormal growth. The species which should redistribute in the strained film have to diffuse through the bulk of the Ni grains [**73**]. In [**74**], it has been suggested that the driving force to operate GG and AGG requires that the surface of the film be free when the film is under compression.

Fig. 9 is a sketch connecting AGG and NGG to GB diffusion. The GBs between OR3 (yellow) and OR1 grains move much faster than the GBs between the two variants of OR1 (blue/pink) and between the OR1 and OR2 grains (blue/green and pink/green). When the capping layer on the film stops surface diffusion, NGG slows down and AGG stops; the anisotropy of mobility of the GBs in a direction parallel to the substrate is related to the anisotropy of diffusion along the GBs. This mechanism can only be efficient if there is a sink or a source at one end of the GB, such as the free surface for thin films on which surface diffusion is the fastest mechanism for redistributing atoms.

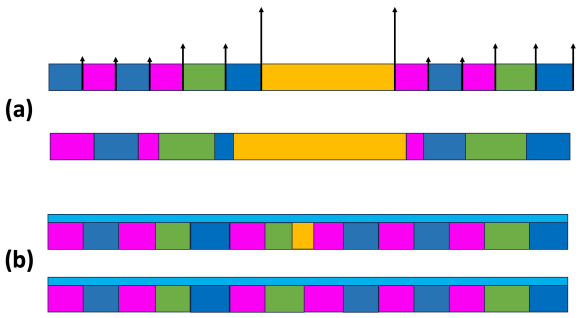

Figure 9. *Sketch of GG in a columnar film (a) without and (b) with capping layer; the arrow length represents the GB diffusion rate. OR3 (100) grains are yellow. OR1 (111) grains are pink or blue and OR2 (111) grains are green. In (a) GBs between OR3 and OR1 move faster than the other GBs because diffusion along them is faster. In (b) GG is sluggish and (100) grains cannot grow.*

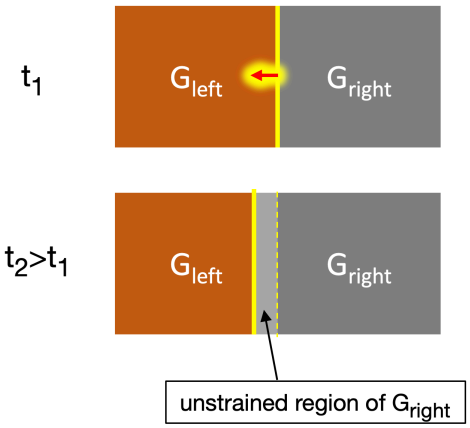

Figure 10. *Sketch showing GB motion as time of annealing increases, because of the asymmetry of strain in the two adjacent grains.*

All the grains in the Ni film are under compressive stress and elastically deformed. To relieve this deformation, among the diffusion mechanisms which are involved, our experiments have shown that GB diffusion is a major player. Fig. 10 visualizes the evolution of strain of a bicrystal due to grain boundary motion in connection with grain boundary diffusion. Locally, the GB is a fast path to relieve the strain in the grains, probably by disconnection motion [**4**], which produces a motion of the GB towards one grain (G_{left} in the sketch). The right grain becomes locally unstrained (or less strained). At its new position, the GB is now surrounded by a stressed grain on one side and an unstrained (or less strained) grain on the other side. Thus, the GB continues to move in the grain which has the highest strain and replaces the swept region by an unstrained piece of grain G_{right}. This decreases the total energy of the two-grain system. The driving force due to the differential stress, produces a GB motion which widens the unstrained (or less strained) region in the right grain.
At the local scale around the GB, the asymmetric elastic deformation of the two grains persists as the GB moves till it has swept the entire left grain and replaced it by an unstrained (or less strained) right grain. This mechanism is similar to the one proposed for DIGM (diffusion induced GB migration) [**75**,**76**] but with a mechanical instead of chemical driving force.
We should stress that this explanation is a conjecture, based on a mechanism of GB motion by disconnections and related to the asymmetric strain of the two grains abutting at the GB. Our experiments do not provide atomistic information to support this mechanism.
In the case of the growth of a (100) grain at the expense of a (111) grain, there is a clear driving force pushing the GB towards the (111) grain: GB moves because the (100) grains have a smaller lateral stress than the (111) grains. AGG can be seen as the reorientation of the (111) grain into a (100) grain with less or no more strain.
In the case of a GB between two (111) grains, the same mechanism stands once the GB has started to move in one of the (111) grains. A slight asymmetry of strain at the local scale around the GB builds-up due to a strain relief in the grain from which the GB moves. One grain has less strain than the other and the GB continues to move in the most strained grain to "replace" it by a less strained or unstrained grain.

5. Summary

100 nm thick Ni thin films with a microstructure containing small (100) grains annealed at and above 1023 K, undergo AGG of (100) grains at the expense of a (111) texture. The GBs between (111) and (100) grains move more than 10 times faster than the GBs between the (111) grains. A controlled microstructure of the film is provided by using a (0001) sapphire substrate. It allows an analysis of grain growth in self-similar microstructure at different temperatures.

AGG in these films stops when they are capped by an oxide layer, i.e., when surface diffusion is stopped. In addition, NGG slows down. Thus, it is suggested that diffusion along the GB accelerates the release of the thermal strain induced by the difference in thermal expansion between the film and the substrate. The anisotropy of diffusion along the GBs allows the grains which contain less strain to grow at the expense of the others. If the mechanism of growth involving GB diffusion is inhibited GG has to proceed through bulk diffusion which gives no advantage to AGG.

The Ni grains have preferred ORs on c-sapphire: most of them exhibit the usual OR1 at low temperature with a few grains in OR2. A new OR3 in which the alignment on the densest directions of the c-plane of sapphire is not the <011> densest direction in the (100) plane but a <010> direction. This OR has also been found recently in thin films of high entropy alloys.

Acknowledgements

The authors thank A. Savan for deposition of the Ni on c-sapphire, S. Mohan Das for helping with the nano-diffraction of Ni films, and V. Heresanu for X-ray measurement on the as-deposited Ni films. The authors gratefully acknowledge P. Wynblatt, N. Bozzolo and U. Dahmen for enlightening discussions. GD and SA are thankful for support by the Deutsche Forschungsgemeinschaft (DFG) within project B06 of Collaborative Research Center (SFB) 1394 “Structural and Chemical Atomic Complexity - from defect phase diagrams to material properties”, project number 409476157.

References

[1] A. Bhattacharya, Y.-F. Shen, C.M. Hefferan, S.F. Li, J. Lind, R.M. Suter, C.E. Krill III, G.S. Rohrer, Grain boundary velocity and curvature are not correlated in Ni polycrystals, Science 374 (2021) 189-193. DOI: 10.1126/science.abj3210

[2] Z. Xu, Y.-F. Shen, S.K. Naghibzadeh, X. Peng, V. Muralikrishnan, S. Maddali, D. Menasche, A.R. Krause, K. Dayal, R.M. Suter, G.S. Rohrer, Grain boundary migration in polycrystalline α-Fe, Acta Mater. 264 (2024) 119541. DOI: 10.1016/j.actamat.2023.119541

[3] C.E. Krill III, E.A. Holm, J.M. Dake, R. Cohn, K. Holikova, F. Andorfer, Extreme abnormal grain growth: connecting mechanisms to microstructural outcomes, Annu. Rev. Mater. Res. 53 (2023) 319-345. DOI: 10.1146/annurev-matsci-080921-091647

[4] J. Han, S.L. Thomas, D.J. Srolovitz, Grain-boundary kinetics: a unified approach, Prog. Mater. Sci. 98 (2018) 386-476. DOI: 10.1016/j.pmatsci.2018.05.004

[5] M. Winning, G. Gottstein, L.S. Shvindlerman, On the mechanisms of grain boundary migration, Acta Mater. 50 (2002) 353–363. DOI: 10.1016/S1359-6454(01)00343-3

[6] C. Herring, Surface tension as a motivation for sintering. In: Gomer R et al., editors. The physics of powder metallurgy. New York (NY): McGraw-Hill; 1949.

[7] S. Florez, K. Alvarado, B. Murgas, N. Bozzolo, D. Chatain, C.E. Krill III, M. Wang, G.S. Rohrer, M. Bernacki, Acta Mater. 222 (2022) 117459. DOI: 10.1016/j.actamat.2021.117459

[8] M. Verma, S. Sugathan, S. Bhattacharyya, R. Mukherjee, Effect of concurrent thermal grooving and grain growth on morphological and topological evolution of a polycrystalline thin film: Insights from a 3D phase-field study. Acta Mater. 261 (2023) 119393 DOI: 0.1016/j.actamat.2023.119393

[9] F.Y. Génin, W.W. Mullins, P. Wynblatt, Capillary instabilities in polycrystalline metallic foils: Experimental observations of thermal pitting in nickel, Acta Metall. Mater. 40 (1992) 3239. DOI: 10.1016/0956-7151(94)90167-8

[10] P.R. Gadkari, A.P. Warren, R.M. Todi, R.V. Petrova, K.R. Coffey, Comparison of the agglomeration behavior of thin metallic films on SiO_2, J. Vac. Sci. Technol. A 23 (2005) 1152-1161. DOI: 10.1116/1.1861943

[11] U. Dahmen, K.H. Westmacott, TEM characterization of grain boundaries in mazed bicrystal films of aluminum, MRS Proc. 229 (1991) 167. DOI: 10.1557/ PROC- 229- 167.

[12] D. Chatain, B. Courtois, I. Ozerov, N. Bozzolo, M. Kelly, G.S. Rohrer, P. Wynblatt, Growth and orientation relationships of Ni and Cu films annealed on slightly miscut (1-102) r-sapphire substrates, J. Cryst. Growth, 508 (2019) 24-33. DOI: 10.1016/j.jcrysgro.2018.11.024

[13] A. Pugliese, B. Shyam, G. M. Repa, A.H. Nguyen, A. Mehta, E.B. Webb III, L.A. Fredin, N.C. Strandwitz, Atomic-Layer-Deposited aluminum oxide thin films probed with X-ray scattering and compared to molecular dynamics and density functional theory models, ACS Omega 7 ***(*2022)** 41033-41043, DOI: 10.1021/acsomega.2c04402

[14] V. Cremers, R.L. Puurunen, J. Dendooven, Conformality in atomic layer deposition: Current status overview of analysis and modelling Appl. Phys. rev. 6 (2019) 021302. DOI: 10.1063/1.5060967

[15] P. Roy, C. Badie, J.B. Claude, A. Barulin, A. Moreau, J. Lumeau, M. Abbarchi, L. Santinacci, J. Wenger, Aluminum metasurface with hybrid multipolar plasmons for 1000-fold broadband visible fluorescence enhancement and multiplexed biosensing, ACS Appl. Nano Mater. 4 (2021) 7199-7205. DOI: 10.1021/acsanm.1c01160

[16] S.W. Hieke, B. Breitbach, G. Dehm, C. Scheu, Microstructural evolution and solid state dewetting of epitaxial Al thin films on sapphire (α-Al_2O_3), Acta Mater. 133 (2017) 356-366. DOI: 10.1016/j.actamat.2017.05.026

[17] J. Ye, C.V. Thompson, Anisotropic edge retraction and hole growth during solid-state dewetting of single crystal nickel thin films, Acta Mater. 59 (2011) 582-589. DOI: 10.1016/j.actamat.2010.09.062

[18] G.H. Kim, C.V. Thompson, Effect of surface energy anisotropy on Rayleigh-like solid-state dewetting and nanowire stability, Acta Mater. 84 (2015) 190-201. DOI: 10.1016/j.actamat.2014.10.028

[19] J.A. Thornton, The microstructure of sputter-deposited coatings, J. Vac. Sci. Technol. A4 (1986) 3059-3065. DOI: 10.1116/1.573628

[20] G. Dehm, H. Edongué, T. Wagner, S.H. Oh, E. Arzt, Obtaining different orientation relationships for Cu films grown on (0001) α-Al_2O_3 substrates by magnetron sputtering, Z. Metallkunde, 96 (2005) 249-254. DOI: 10.3139/146.101027

[21] D.L. Medlin, K.F. McCarty, R.Q. Hwang, S.E. Guthrie, M.I. Baskes, Orientation relationships in heteroepitaxial aluminum films on sapphire**,** Thin Solid Films 299 (1997) 110-114. DOI: 10.1016/S0040-6090(96)09393-5

[**22]** S. Ahmad, T. Brink, C.H. Liebscher, G. Dehm, Influence of variation in grain boundary parameters on the evolution of atomic structure and properties of [111] tilt boundaries in aluminum. Acta Mater. (2024) 119732. DOI: 10.1016/j.actamat.2024.119732

[23] R.F. Sekerka, Equilibrium and growth shapes of crystals: how do they differ and why should we care? Crystal Research &Technology, 40 (2005) 291-306. DOI: 10.1002/crat.200410342

[24] N. Thangaraj, K.H. Westmacott, U. Dahmen, Epitaxial growth of (001) Al on (111) Si by vapor deposition, Appl. Phys. Lett. 61 (1992) 913-915. DOI: 10.1063/1.107726.

[25] F. Genin, W. Mullins, P. Wynblatt, Capillary instabilities in polycrystalline metallic foils: Experimental observations of thermal pitting in nickel, Acta Metall. Mater. 42 (1994) 1489-1492. DOI: 10.1016/0956-7151(94)90167-8

[26] U. Erb, W. Abel, H. Gleiter, The significance of atomic matching for the structure of interphase boundaries, Scripta Metall. 16 (1982) 1317-1319. DOI: 10.1016/0036-9748(82)90418-5

[27] H. J. Fecht, H. Gleiter, Lock-in model for the atomic structure of interphase boundaries between metals and ionic crystals, Acta metall. 33 (1985) 551-562. DOI: 10.1016/0001-6160(85)90019-7

[28] R. Maurer, H.F. Fischmeister, Low energy heterophase boundaries in the system silver-nickel and in other weakly bonded systems, Acta Metall. 37 (1989) 1177-l189. DOI: 10.1016/0001-6160(89)90113-2

[29] H. Meltzman, D. Mordehai, W.D. Kaplan, Solid-solid interface reconstruction at equilibrated Ni-Al_2O_3 interfaces, Acta Mater. 60 (2012) 4359-4369. DOI: 10.1016/j.actamat.2012.04.037

[30] A.A. Taylor, S.H. Oh, G. Dehm, Microplasticity phenomena in thermomechanically strained nickel thin films, J. Mater. Sci. 45 (2010) 3874-3881. DOI: 10.1007/s10853-010-4445-0

[31] R.F.C. Farrow, G.R. Harp, R.F. Marks, T.A. Rabedeau, M.F. Toney, D. Weller, S.S.P. Parkin, Epitaxial growth of Pt on basal-plane sapphire: a seed film for artificially layered magnetic metal structures, J. Cryst. Growth, 133 (1993) 47-58. DOI: 10.1016/0022-0248(93)90102-3

[32] Z. Fogarassy, G. Dobrik, L.K. Varga, L.P. Biró, J.L. Lábár, Growth of Ni layers on single crystal sapphire substrates, Thin Solid Films, 539 (2013) 96-101. DOI: 10.1016/j.tsf.2013.05.077

[33] H. Bialas, E. Knoll**,** Heteroepitaxy of copper on sapphire under UHV conditions**,** Vacuum**,** 45 **(**1994**)** 959-966**.** DOI: 10.1016/0042-207X(94)90220-8

[34] Y. Addab, M.K. Kini, B. Courtois, A. Savan, A. Ludwig, N. Bozzolo, C. Scheu, G. Dehm, D. Chatain, Microstructure evolution and thermal stability of equiatomic CoCrFeNi thin films on (0001) α-Al_2O_3, Acta Mater. 200 (2020) 908-921. DOI: 10.1016/j.actamat.2020.09.064

[35] M.K. Kini, S. Lee, A. Savan, B. Breitbach, J.P. Best, M.Ghidelli, C. Scheu, A. Ludwig, D. Chatain, G. Dehm, Equiatomic CoCrFeNi thin films on c-sapphire: orientation relationships and the role of twins, Advanced Engineering Materials (2024) 2400720. DOI: 10.1002/adem.202400720

[36] J.A. Floro, C.V. Thompson, R. Carel, P.D. Bristowe, Competition between strain and interface energy during epitaxial grain growth in Ag films on Ni(001), J. Mater. Res. 9 (1994) 2411-2424. DOI: 10.1557/JMR.1994.2411

[37] D. Chatain, P. Wynblatt, A.D. Rollett, G.S. Rohrer, Importance of interfacial step alignment in hetero-epitaxy and orientation relationships: the case of Ag equilibrated on Ni substrates. Part 2 experiments, J. Mater. Sci. 50 (2015) 5276-5285. DOI: 10.1007/s10853-015-9075-0

[38] D. Chatain, P. Wynblatt, Importance of interfacial step alignment in hetero-epitaxy and orientation relationships: the case of Ag equilibrated on Ni substrates. Part 1 computer simulations, J. Mater. Sci. 50 (2015) 5262-5275. DOI: 10.1007/s10853-015-9074-1

[39] P. Wynblatt, D. Chatain, A.D. Rollett, U. Dahmen, Origin of an unusual systematic variation in the heteroepitaxy of Ag on Ni - the roles of twinning and step alignment, Acta Mater. 168 (2019) 121-132. DOI: 10.1016/j.actamat.2019.01.049

[40] S. Ramamurthy, C.B. Carter, The {111}/{100} Interface in cubic materials and related systems, Phys. Stat. Sol. (a) 166 (1998) 37-55. DOI: 10.1002/(SICI)1521-396X(199803)166:1<37::AID-PSSA37>3.0.CO;2-W

[41] D. Wolf, Reconstruction of NaCl surfaces from a dipolar solution to the Madelung problem, Phys. Rev. Lett. 68, (1992) 3315. DOI: 10.1103/PhysRevLett.68.3315

[42] W.E. Lee, K.P.D. Lagerlof, Structural and electron diffraction data for sapphire (α-Al_2O_3), J. Electron Microsc. Tech. 2 (1985) 247-258. DOI: 10.1002/jemt.1060020309

[43] J.A. Floro, C.V. Thompson, R. Carel, P.D. Bristowe, Competition between strain and interface energy during epitaxial grain growth in Ag films on Ni(001), J. Mater. Res. 9 (1994) 2411-2424. DOI: 10.1557/JMR.1994.2411

[44] C.V. Thompson, R. Carel, Stress and grain growth in thin films, J. Mech. Phys. Solids, 44 (1996) 657-671. DOI 10.1016/0022-5096(96)00022-1

[45] C.V. Thompson, R. Carel, Grain growth and texture evolution in thin films, Materials Science Forum, 204–206 (1996) 83–98. DOI: 10.4028/www.scientific.net/msf.204-206.83.

[46] P. Sonnweber-Ribic, P. Gruber, G. Dehm, E. Arzt, Texture transition in Cu thin films: Electron backscatter diffraction vs. X-ray diffraction, Acta Mater. 54 (2006) 3863-3870. DOI: 10.1016/j.actamat.2006.03.057

[47] R. Carel, Ph D thesis, Massachussetts Institute of Technology, 1995.

[48] G. Dehm, T.J. Balk, H. Edongué, E. Arzt, Small-scale plasticity in thin Cu and Al films, Microelectron Eng. 70 (2003) 412-424. DOI: 10.1016/S0167-9317(03)00395-2

[49] G. Dehm, T.J. Balk, B. von Blanckenhagen, P. Gumbsch, E. Arzt, Dislocation dynamics in sub-micron confinement: recent progress in Cu thin film plasticity, Z. Metallkde. 93 (2002) 383-391. DOI: 10.3139/146.020383

[50] H.M. Ledbetter, R.P. Reed, Elastic properties of metals and alloys, I. Iron, Nickel, and Iron-Nickel alloys, J. Phys. Chem. Ref. Data 2. *(*1973) 531-618. DOI: 10.1063/1.3253127

[51] W.M. Haynes, D.R. Lide, T.J. Bruno, CRC handbook of chemistry and physics, CRC handbook of chemistry and physics: a ready-reference book of chemical and physical data. 2016-2017, 97th Ed. / Boca Raton, Florida, CRC Press.

[52] W.M. Yim, R.J. Paff, Thermal expansion of AlN, sapphire, and silicon, J. Appl. Phys. 45 (1974) 1456-1457. DOI: 10.1063/1.1663432.

[53] W.D. Nix, Mechanical properties of thin films, Metall. Mater. Trans. B 20 (1989) 2217-2245. DOI: 10.1007/BF02666659

[54] S. Curiotto, H. Chien, H. Meltzman, P. Wynblatt, G.S. Rohrer, W.D. Kaplan, D. Chatain, Orientation relationships of copper crystals on c-plane sapphire, Acta Mater. 59 (2011) 5320-5331. DOI: 10.1016/j.actamat.2011.05.008

[55] H. Meltzman, D. Chatain, D. Avizemer, T.M. Besmann, W.D. Kaplan, The equilibrium shape of nickel, Acta Mater. 59 (2011) 3473-3483. DOI: 10.1016/j.actamat.2011.02.021

[56] D. Chatain, V. Ghetta, P. Wynblatt, Equilibrium shape of copper crystals grown on sapphire, Interface Sci. 12 (2004) 7-18. DOI: 10.1023/B:INTS.0000012290.07441.a8

[57] J.C. Heyraud, J.J. Métois, Equilibrium shape and temperature; Lead on graphite, Surf. Sci. 128 (1983) 334-342. DOI: 10.1016/S0039-6028(83)80036-3

[58] A. Emundts, H.P. Bonzel, P. Wynblatt, K. Thurmer, J. Reutt-Robey, E.D. Williams, Continuous and discontinuous transitions on 3D equilibrium crystal shapes: a new look at Pb and Au, Surf. Sci. 481 (2001) 13-24. DOI: 10.1016/S0039-6028(01)01055-X

[59] V.K. Kumikov, K.B. Khokonov, On the measurement of surface free energy and surface tension of solid metals, J. App. Phys. 54 (1983) 1346-1350. DOI: 10.1063/1.332209

[60] B.J. Keene, Review of data for the surface tension of pure metals, Int. Mater. Rev. 38 (1993) 157-192. DOI: 10.1179/imr.1993.38.4.157

[61] F. Farzam, B. Bellón, D. Chatain, J.A. Jiménez, B. Breitbach, M. Ghidelli, M.J. Duarte, G. Dehm, Decomposition and dewetting of super-saturated Cu-15at.% Co solid solution film, Materials & Design, 241 (2024) 112892. DOI: 10.1016/j.matdes.2024.11289

[62] J.M. Blakely, H. Mykura, Self diffusion measurements on nickel by the mass transfer method, Acta Metall. 9 (1961) 23-31. DOI:10.1016/0001-6160(61)90034-7

[63] P.S. Maiya, J.M. Blakely, Surface self-diffusion and surface energy of nickel, J. Appl. Phys. 38 (1967) 698-704. DOI: 10.1063/1.1709399

[64] H.P. Bonzel, E.E. Latta**,** Surface self-diffusion on Ni(110): Temperature dependence and directional anisotropy, Surf. Sci. 76 (1978) 275-295. DOI: 10.1016/0039-6028(78)90098-5

[65] B. Yao, T. Sun, V. Kumar, K. Barmak, K. Coffey, Grain growth and void formation in dielectric-encapsulated Cu thin films, J. Mater. Research, 23 (2008) 2033-2039. DOI: 10.1557/JMR.2008.0254

[66] G. Gottstein, L.S. Schvindlerman, On the true dependence of grain boundary migration rate on driving force, Scripta Metall. Mater. 27 (1992) 1521-1526. DOI: 10.1016/0956-716X(92)90138-5

[67] M. Winning, G. Gottstein, L. S. Shvindlerman, Stress induced grain boundary motion, Acta mater. 49 (2001) 211-219. DOI: 10.1016/S1359-6454(00)00321-9

[**68**] R. Treml, D. Kozic, J. Zechner, X. Maeder, B. Sartory, H.-P. Gänser, R. Schöngrundner, J. Michler, R. Brunner, D. Kiener, High resolution determination of local residual stress gradients in single- and multilayer thin film systems, Acta Mater. 103 (2016) 616–623. DOI: 10.1016/j.actamat.2015.10.044

[69] R. Dannenberg, E.A. Stach, J.R. Groza, B.J. Dresser, TEM annealing study of normal grain growth in silver thin films, Thin Solid Films, 379 (2000) 133-138. DOI: 10.1016/S0040-6090(00)01570-4

[70] L. Han, Lars P.H. Jeurgens, C. Cancellieri, J. Wang, Y. Xu, Y. Huang, Y. Liu, Z. Wang, Anomalous texture development induced by grain yielding anisotropy in Ni and Ni-Mo alloys, Acta Mater. 200 (2020) 857–868. DOI: 10.1016/j.actamat.2020.09.063

[71] M.J. Kobrinsky, C.V. Thompson, The thickness dependence of the flow stress of capped and uncapped polycrystalline Ag thin films, Appl. Phys. Lett. 73 (1998) 2429-2431. DOI: 10.1063/1.122471

[72] D. Weiss, O. Kraft, E. Arzt, Grain-boundary voiding in self-passivated Cu-1at.% Al alloy films on Si substrates, J. Mater. Res. 17 (2002) 1363-1370. DOI: 10.1557/JMR.2002.0203

[73] K.N.Tu, Irreversible processes of spontaneous whisker growth in bimetallic Cu-Sn thin-film reactions, Phys. Rev. B, 49 (1994) 2030-2035. DOI: 10.1103/PhysRevB.49.2030

[74] O. Glushko, G. Dehm, Initiation and stagnation of room temperature grain coarsening in cyclically strained gold films, Acta Mater. 169 (2019) 99-108. DOI: 10.1016/j.actamat.2019.03.004

[75] J.W. Cahn, J.D. Pan, R.W. Balluffi, Diffusion induced grain boundary migration, Scripta Metallurgica. 13 (1979) 503–509. DOI: 10.1016/0036-9748(79)90078-4

[76] R.W. Balluffi, J.W. Cahn, Mechanism for diffusion induced grain boundary migration**,** Acta Metallurgica**.** 29 (1981) 493-500**.** DOI: 10.1016/0001-6160(81)90073-0